The Discovery and Characterization of ML218: A Novel, Centrally Active T-Type Calcium Channel Inhibitor with Robust Effects in STN Neurons and in a Rodent Model of Parkinson's Disease

Zixiu Xiang,[†,‡,⊥] Analisa D. Thompson,[†,‡,⊥] John T. Brogan,[§,‖] Michael L. Schulte,[§,‖]
Bruce J. Melancon,[‡,‖,⊥] Debbie Mi,[‡,⊥] L. Michelle Lewis,[‡,⊥] Bende Zou,[○] Liya Yang,[○]
Ryan Morrison,[‡,‖,⊥] Tammy Santomango,[‡,⊥] Frank Byers,[‡,⊥] Katrina Brewer,[‡,⊥]
Jonathan S. Aldrich,[‖,⊥] Haibo Yu,[#] Eric S. Dawson,[‡,‖,⊥] Min Li,[#,▽] Owen McManus,[#,▽]
Carrie K. Jones,[‡,⊥] J. Scott Daniels,[‡,‖,⊥] Corey R. Hopkins,[‡,§,‖,⊥] Ximin Simon Xie,[○] P. Jeffrey Conn,[‡,‖,⊥]
C. David Weaver,[‡,‖,⊥] and Craig W. Lindsley*[,‡,§,‖,⊥]

[‡]Department of Pharmacology, [§]Department of Chemistry, [‖]Vanderbilt Specialized Chemistry Center for Accelerated Probe Development (MLPCN), [⊥]Vanderbilt Center for Neuroscience Drug Discovery, Vanderbilt University Medical Center, Nashville, Tennessee 37232-6600, United States

[#]Department of Neuroscience, High Throughput Biology Center, [▽]Johns Hopkins Ion Channel Center (JHICC), Johns Hopkins University, Baltimore, Maryland 21205, United States

[○]AfaSci Research Laboratory, AfaSci, Inc., Redwood, California 94063, United States

S *Supporting Information*

ABSTRACT: T-Type Ca^{2+} channel inhibitors hold tremendous therapeutic potential for the treatment of pain, epilepsy, sleep disorders, essential tremor, and other neurological disorders; however, a lack of truly selective tools has hindered basic research, and selective tools from the pharmaceutical industry are potentially burdened with intellectual property (IP) constraints. Thus, an MLPCN high-throughput screen (HTS) was conducted to identify novel T-type Ca^{2+} channel inhibitors free from IP constraints, and freely available through the MLPCN, for use by the biomedical community to study T-type Ca^{2+} channels. While the HTS provided numerous hits, these compounds could not be optimized to the required level of potency to be appropriate tool

compounds. Therefore, a scaffold hopping approach, guided by SurflexSim, ultimately afforded ML218 (CID 45115620), a selective T-type Ca^{2+} ($Ca_v3.1$, $Ca_v3.2$, $Ca_v3.3$) inhibitor ($Ca_v3.2$, IC_{50} = 150 nM in Ca^{2+} flux; $Ca_v3.2$ IC_{50} = 310 nM; and $Ca_v3.3$ IC_{50} = 270 nM, respectively in patch clamp electrophysiology) with good DMPK properties, acceptable in vivo rat PK, and excellent brain levels. Electrophysiology studies in subthalamic nucleus (STN) neurons demonstrated robust effects of ML218 on the inhibition of T-type calcium current, inhibition of low threshold spike, and rebound burst activity. Based on the basal ganglia circuitry in Parkinson's disease (PD), the effects of ML218 in STN neurons suggest a therapeutic role for T-type Ca^{2+} channel inhibitors, and ML218 was found to be orally efficacious in haloperidol-induced catalepsy, a preclinical PD model, with comparable efficacy to an A_{2A} antagonist, a clinically validated PD target. ML218 proves to be a powerful new probe to study T-type Ca^{2+} function in vitro and in vivo, and freely available.

KEYWORDS: T-Type calcium channel, inhibitor, electrophysiology, Parkinson's disease

Voltage-gated calcium channels (VGCCs) modulate the entry of calcium (Ca^{2+}) into cells in response to depolarization of the membrane and elicit a number of Ca^{2+}-dependent processes.[1] VGCCs are classified as either high-voltage-activated (L-, N-, P/Q-, and R-types) or low-voltage-activated (T-type).[2−7] The "T" in T-type Ca^{2+} channels refers to their characteristic transient, or fast, inactivation of the channel and small conductance.[2−8] Molecular cloning studies have identified three genes (*CACNA1G*, *CACNA1H*, *CACNA1I*) encoding the main pore-forming α1 subunit resulting in three members in the T-type calcium channel

family: $Ca_v3.1$ (α1G), $Ca_v3.2$ (α1H), and $Ca_v3.3$ (α1I).[2−10] All three Ca_v3 family members are heterogeneously expressed in the brain and many peripheral organs such as the heart and vascular smooth muscle. A wealth of literature suggests that subtype-selective Ca_v3 modulators should produce more specific pharmacological actions for a variety of neurological, psychiatric,

Figure 1. First generation T-type Ca^{2+} inhibitors derived from marketed antiepileptic **1** and **2**, antihypertensives **3** and **4**, neuroleptic **5**, and antipsychotic **6** drugs.

and cardiovascular disorders (such as epilepsy, pain, movement disorders, hearing loss, sleep/wake states, cancer, and overactive bladder) with fewer side effects than *pan*-Ca^{2+} channel inhibitors.[2−11] Importantly, T-type Ca^{2+} channels are strongly associated with rhythmic firing patterns in key brain regions within the CNS.[2−11] For example, $Ca_v3.1$ T-type calcium channels are present in the olivocerebellar system, and inhibitors could block tremor-rhythm generation, suggesting potential therapeutic potential for essential tremor.[12−16] This postulate has been borne out in both preclinical models of essential tremor as well as in the clinic with zonisamide (ZNS) and lamotrigine, antiepileptic drugs possessing T-type calcium channel inhibitory activity in addition to blockade of voltage-gated Na^+ channels.[12−16] This could also be extended to the basal ganglia circuit, where abnormal burst firing results in overactivation of the indirect pathway, leading to Parkinsonian tremors,[17−20] and this is where our interest in this target resides. However, the therapeutic potential of T-type calcium channels has been hampered by both a lack of truly selective, central active small molecule tools and, in the case of exceptional tool compounds, intellectual property constraints.

The first generation of T-type Ca^{2+} inhibitors was discovered based on drugs originally developed for other targets (Figure 1). The antiepileptic drugs zonisamide (ZNS) **1** and ethosuximide **2** were found to inhibit T-type calcium channel at therapeutic concentrations.[20,21] Roche later identified the dual T-/L-type calcium channel antagonist mibefradil **3**, which was briefly marketed as an antihypertensive agent.[22,23] Studies have shown that **3** is a potent T-type inhibitor with 10- to 30-fold selectivity for T- over L-type Ca^{2+} channels. Therefore, it has been widely used as a pharmacological tool for studying T-type Ca^{2+} channels.[22,23] However, mibefradil has poor penetration into CNS. Similarly, efonidipine **4** was also shown to preferentially inhibit T- over L-type Ca^{2+} channels.[24] Shortly thereafter, the neuroleptic agent flunazirine **5**[25] and the antipsychotic pimozide **6**[26] were shown to inhibit (Ca_v3 $IC_{50}s$ ∼ 600 nM) or bind (K_i ∼ 40 nM) to T-type Ca^{2+} channels; however, both were far more potent against biogenic amine targets. While these tools provided modest advances in our understanding of T-type Ca^{2+} channels, they did provide evidence that inhibition of T-type Ca^{2+} channels in man was well tolerated upon both acute and chronic dosing with **1-6**.[20−26]

The majority of the second generation T-type Ca^{2+} inhibitors were derived from HTS campaigns in pharmaceutical companies aimed at developing selective T-type Ca^{2+} inhibitors and are covered by patents (Figure 2).[27] Here, the major players of published efforts are Merck, inhibitor series **7−10**, and Korea Institute of Science and Technology, inhibitor series **11**, **13**, and **14**.[28−40] Of these, the Merck series are the most potent, possessing good DMPK profiles and in vivo activity in multiple preclinical models. Interestingly, **7** and **8** are voltage independent, while **9** displays voltage-dependent inhibition. Importantly, there are no reports of inhibitors selective among the Ca_v3 family (all are equipotent on $Ca_v3.1$, $Ca_v3.2$, and $Ca_v3.3$). While compounds **7−15** represent a major advance, they are covered by patents and/or published patent applications that can restrict their use by the broader biomedical research community.[27−40]

■ RESULTS AND DISCUSSION

In 2005, the NIH Molecular Libraries Roadmap launched the Molecular Libraries Screening Center Network (MLSCN), a nationwide consortium of facilities that provide high-throughput small molecule screening of biological targets/pathways for which small molecule tools are unavailable.[41] One such target that lacked the appropriate small molecule tools was, at that time, T-type Ca^{2+} channels, as only **1−6** were known.[20−26] Xie and his colleagues have developed and validated an HTS assay using a FLIPR (fluorescent imaging plate reader).[42] The target and the assay were assigned to the Vanderbilt Specialized Screening Center for GPCRs, Ion Channels and Transporters for primary drug screen to identify novel selective T-type channel inhibitors from the MLSCN compound library.[41] During the course of this initiative, the MLSCN became the Molecular Libraries Production Center Network (MLPCN), with increased medicinal chemistry expertise to develop high quality probes for the biomedical community, of which the Vanderbilt Specialized Chemistry Center and the Johns Hopkins Ion Channel Center are members.[41] Also during this time, the pharmaceutical industry disclosed **7−15**, which not only raised the bar for an impactful T-type Ca^{2+} channel inhibitor probe but also required that our Centers develop a T-type Ca^{2+} channel inhibitor probe free of
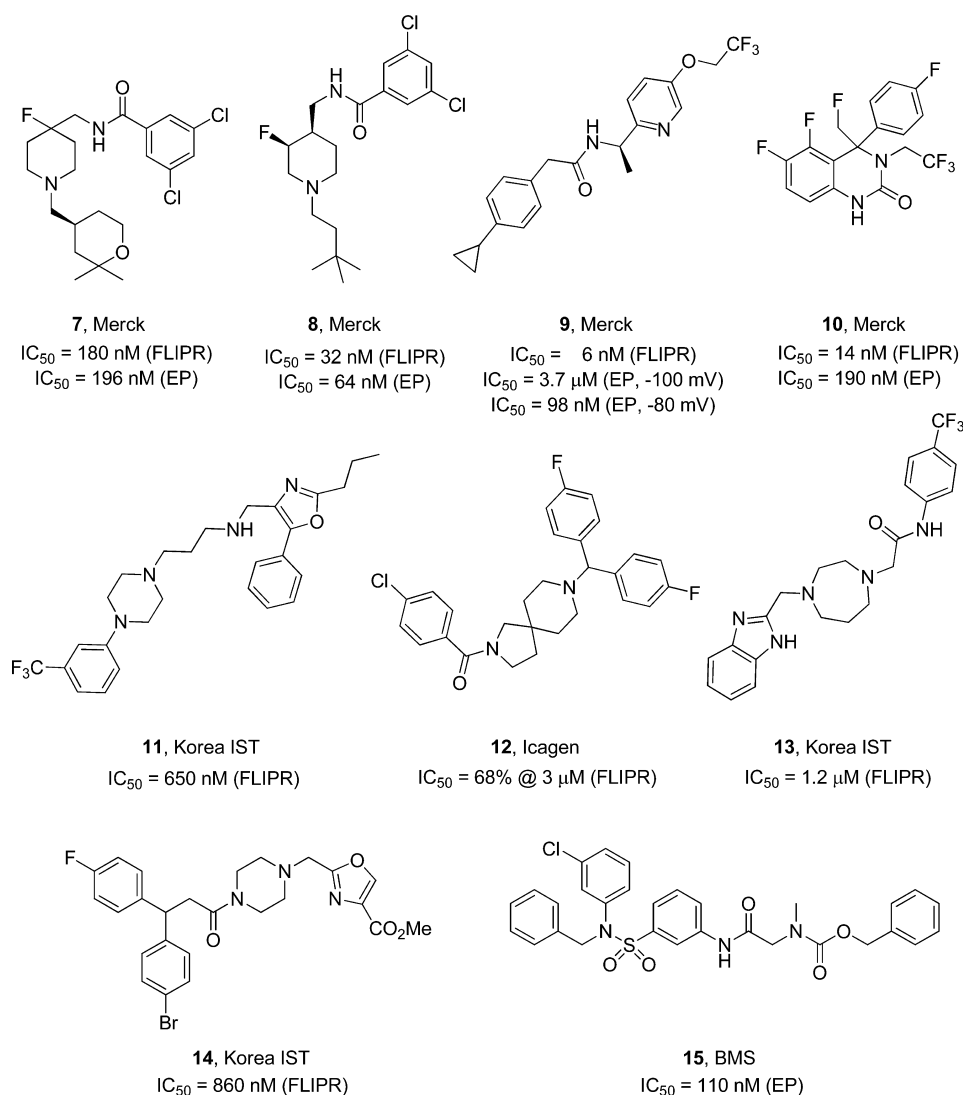
Figure 2. Second generation T-type Ca^{2+} inhibitors **7−15** derived from optimization of HTS hits.

potential IP constraints, of comparable quality to **7−15**, and to be freely available through the MLPCN mechanism for use by the biomedical research community.[27−40]

High-Throughput Screening and Identification of T-Type Ca^{2+} Channel inhibitors. For the discovery of novel T-type Ca^{2+} channel inhibitors, we completed a primary HTS using the 2008 collection of MLSCN library containing 110 720 compounds screened at 10 μM in a single measurement.[41] The primary assay was run against the $Ca_v3.2$ channel expressed in HEK293 cells, and performed in a 384-well format using an FDSS 6000 kinetic imaging plate measuring Ca^{2+} fluorescence. Data quality was controlled by the known T-type Ca^{2+} channel inhibitor **8**[29] as the positive control and the 0.1% DMSO vehicle as the negative control. The assay quality control used a screening window coefficient "Z-factor". The Z' values were between 0.6 and 0.8, indicating excellent assay quality. Primary data analysis was performed by comparing the activity of any test compound with all the other test compounds on the same plate, taking the ratio max in the kinetic time window of 12−40 s with 0−1 s as the baseline. Primary hits were defined as any outliers that were different from all the others based on a z-score threshold of 3, which resulted in 4246 hits. For the confirmation screen, 890 hits were available from Biofocus-DPI and tested with full concentration−response curves

(CRCs), validating only seven hits as $Ca_v3.2$ inhibitors from the primary screen. A counter-screen with the parental HEK line, with native Ca^{2+} channels, presumably both L- and N-type Ca^{2+} channels, indicated that only one confirmed hit was selective for T-type Ca^{2+} channels, **16** (CID3373841), with an IC_{50} of 2.5 μM (Figure 3). Moreover, this represented a new T-type Ca^{2+} inhibitor chemotype and was only active in 23/440 MLPCN assays (never for an ion channel), suggesting minimal promiscuous pharmacology and a good starting point for chemical lead optimization.[43]

Chemical Optimization of 16 (CID3373841). The modular nature of **16**, coupled with the commercial availability of 2-amino oxadiazole monomers led to a two-dimensional library (Figure 4) of 56 analogues, wherein the western aryl moiety and the eastern amide moiety of **16** were varied. All analogues were screened in full CRC in the kinetic Ca^{2+} fluorescence assay. Structure−activity-relationship (SAR) was rather flat, with the best analogue **17** possessing an IC_{50} of 1.1 μM, ~10-fold less potent than the best known inhibitors **7−15**. Evaluation of **17** in Ca_v3 patch electrophysiology (EP) experiments demonstrated an ~10-fold right-shift in potency ($Ca_v3.2$ IC_{50} = 13.5 μM and $Ca_v3.3$ IC_{50} = 11.5 μM), affording weak inhibition of T-type Ca^{2+} channels and far from a high quality MLPCN probe for this target.
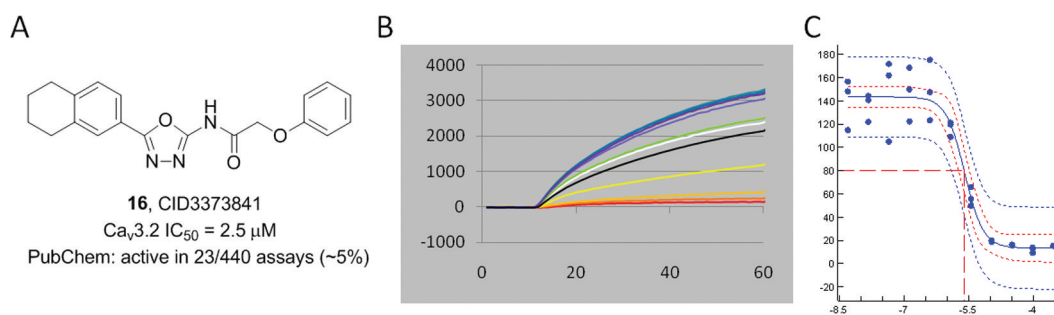
Figure 3. Confirmed HTS hit **16**. (A) Structure of **16**, CID3373841. (B) Raw fluorescence-based HTS assay traces. (C) CRC from fluorescence-based assay (IC$_{50}$ = 2.5 μM).
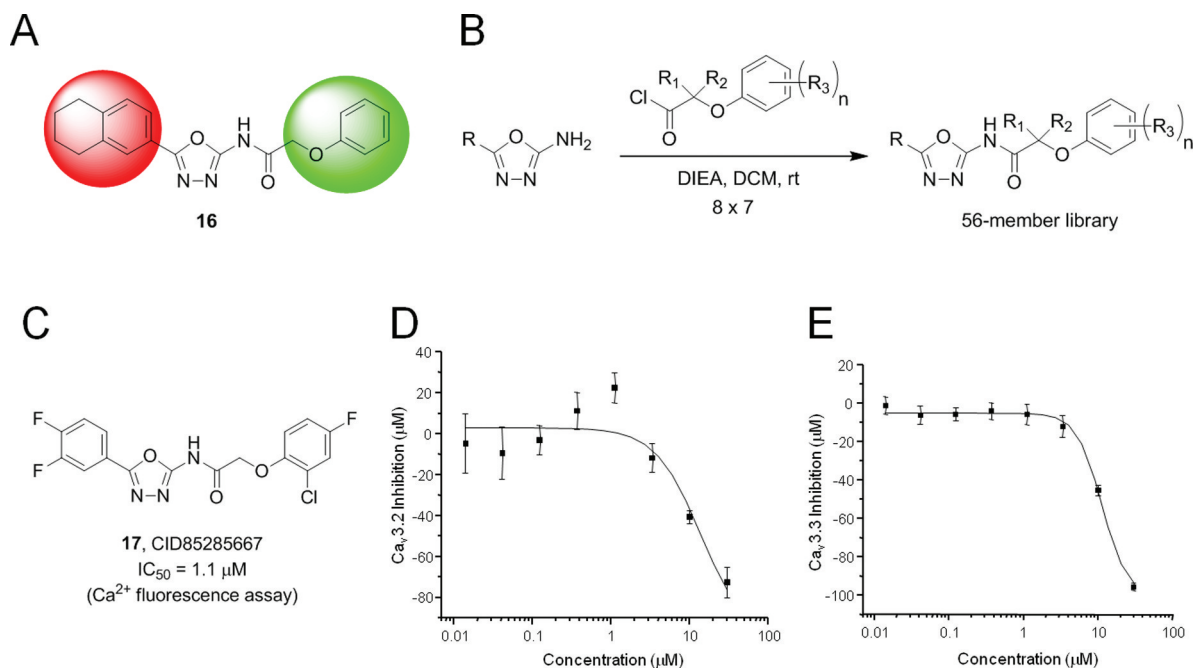
Figure 4. (A) Chemical optimization plan for **16**, a two-dimensional library. (B) 8 × 7 member library design that generated 56 analogues of **16**. (C) Structure of **17** (CID85285667), the most potent analogue with an IC$_{50}$ of 1.1 μM in the Ca^{2+} fluorescence assay. (D) Ca$_{v}$3.2 IonWorks Quattro (patch EP) CRC IC$_{50}$ = 13.5 μM. (E) Ca$_{v}$3.3 IonWorks Quattro (patch EP) CRC IC$_{50}$ = 11.5 μM.

While studying a molecular model of **17** and comparing it to a model of Merck's **8**, it appeared as though the oxadiazole moiety of **17** could be mimicking the piperidine spacer element in **8**, although poorly in this case due to the presence of western aryl ring. Therefore, we prepared a second generation library of analogues (Figure 5) in which the western aryl group in **17** was replaced with branched aliphatic moieties to more closely align with Merck's **8**.[29] A sub-micromolar inhibitor **18** (CID46943243, IC$_{50}$ = 810 nM) resulted, but was still not potent enough to meet target criteria. A SurflexSim[44] morphological similarity algorithm was used to perform multiple flexible alignments of **18** with Merck's **8**, which suggested that the oxadioazole moiety was in fact mimicking the piperidine ring, but the hydrogen bond donors/acceptors of the amide moieties were not properly aligned (Figure 5D). Moreover, patch EP with **18** still displayed a significant right-shift in potency that decreased enthusiasm for continued optimization efforts within this scaffold.

Based on the overall profile of Merck's **8** and the overlay with **18**, we decided to "scaffold hop" around Merck's **8** to access patent-free space and hopefully a more potent T-type Ca^{2+} channel inhibitor probe.[29] Thus, we explored patent databases,

and in conjunction with molecular modeling, identified two potential scaffolds to explore that would be free of IP issues, if we could engender good T-type Ca^{2+} channel activity. The first was based on a 3-amino piperdine scaffold (Figure 6). Employing solution phase parallel synthesis, we quickly constructed two, 12-member libraries (six with the (R)-enantiomer **19** and six with the (S)-enantiomer **20**) wherein the secondary piperdinyl nitrogen was substituted with either a benzyl group or a tert-butyl ethyl moiety and the exocyclic primary amine was acylated with a variety of acid chlorides to deliver analogue libraries **21** and **22**. This effort provided only one active compound, **23** (CID45115608), the (S)-enantiomer with an IC$_{50}$ of 2.4 μM. Interestingly, the (R)-enantiomer (CID45115614) was devoid of activity.

In parallel, we were advancing a [3.1.0] scaffold, wherein modeling suggested we need the (1R,5S,6S) stereochemistry about the 3-azabicylco[3.1.0]hexan-6ylmenthanamine core **24**. As in the Merck series containing **8**,[29] the 3,5-dichlorobenza-mide was optimal; thus, we held that moiety constant in our first generation library and surveyed eight different alkyl groups on the secondary nitrogen. Thus, acylation of **24** with 3,5-dichlorobenzoyl chloride produced **25**. Deprotection of the Boc
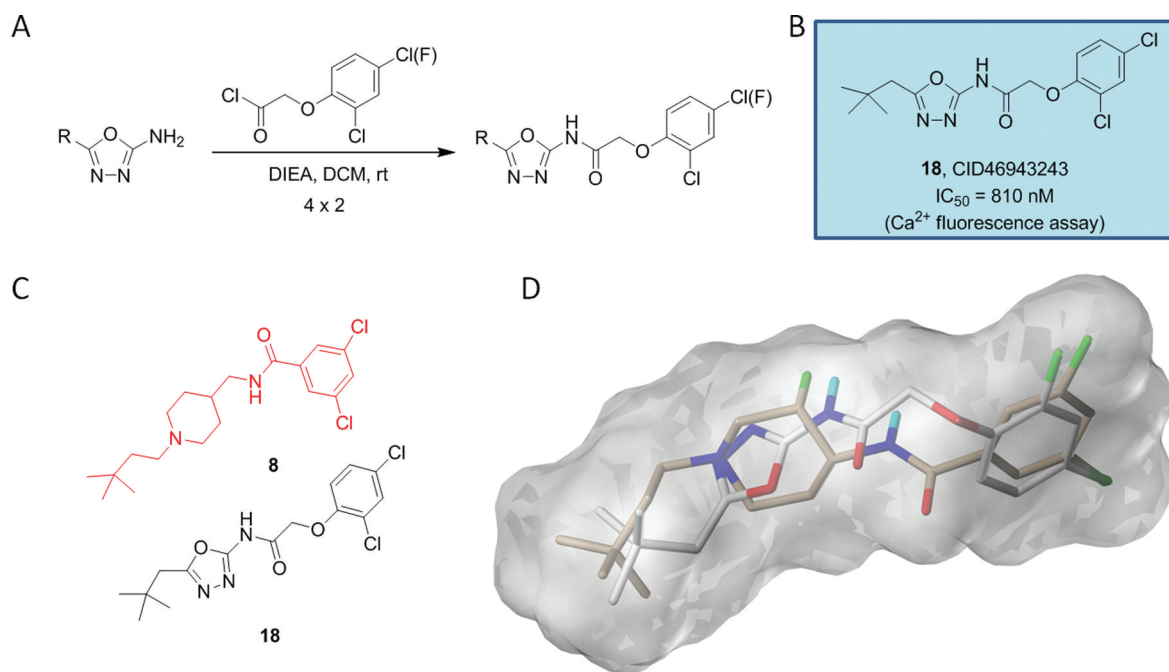
Figure 5. Second generation library of analogues of **17**. (A) 4 × 2 library of branched alkyl analogues. (B) Structure and activity of most potent analogue, **18** (CID46943243). (C) Manual overlay of **18** with Merck's **8**. (D) SurflexSim flexible alignment of **18** (gray) with Merck's **8** (tan), affording reasonable overlap except for amide HBD/HBA.
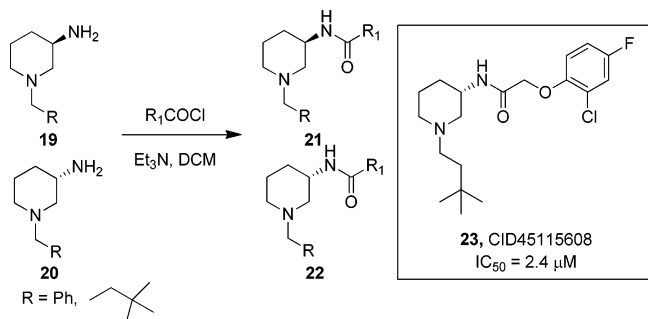

Figure 6. Initial "scaffold hopping" library. 24-membered library of 3-amino piperidine "scaffold hopping" libraries leading to **23** (CID45115608), displaying enantiospecific T-type Ca²⁺ channel inhibition.

group and standard reductive amination delivered analogues **26** (Scheme 1). This library proved far more productive than the 3-aminopiperidine series. Here, four of eight analogues (Figure 7) had potent T-type Ca²⁺ channel inhibitory activity, with **26b** (CID45115620) possessing activity comparable to Merck's **8**[29] with an IC_{50} of 150 nM. Now, a SurflexSim[44] flexible alignment of **26b** with Merck's **8** and **18** provides almost perfect placement of key groups due to the conformational lock of the boat orientation of the enantiopure [3.1.0] ring system (Figure 7B), which is clearer in Figure 7C, showing overlay of **8** and **26b** alone. The potency of **26b** confirmed in patch EP, with a $Ca_v3.2$ IC_{50} of 310 nM and a $Ca_v3.3$ IC_{50} of 274 nM (Figure 8), and in excellent agreement with the Ca²⁺ fluorescence data. Thus, **26b**, derived via "scaffold hopping", was declared an MLPCN probe and assigned ML218.[41] Importantly, ML218 and related structures are not covered under any issued patent or patent application; therefore, the MLPCN probe, ML218, is free of any use restrictions.

Ancillary Pharmacology and DMPK Profiling of ML218. Ancillary pharmacology is a major concern and an issue that plagued both the first and second generation of T-type Ca²⁺ channel inhibitors.[20−40] The original Merck HTS hit was a *des*-fluoro analogue of **8**, which was a potent T-type Ca²⁺ channel inhibitor, but the basic pK_a (8.7) of the piperdinyl nitrogen, in combination with lipophillic moieties at both termini, led to promiscuous ion channel and GPCR pharmacology.[29] To circumvent this, the installation of the *cis-β*-fluoroamine in **8** maintained T-type Ca²⁺ channel inhibition, but attenuated amine bascitiy (pK_a = 7.9) to a degree where ancillary pharmacology significantly improved.[29] Due to modest inductive effects of the π-character of the cyclopropyl ring of the [3.1.0] system, the pK_a (8.1) of the bicyclic nitrogen was also diminished, relative to a piperidine nitrogen, but to a lesser degree than the *cis-β*-fluoroamine in **8**.[29] However, even this subtle diminution in pK_a translated to a clean ancillary pharmacology profile for ML218. To more fully characterize this novel Ca_v3 inhibitor probe molecule, ML218 was tested in Ricerca's Lead Profiling Screen (binding assay panel of 68 GPCRs, ion channels, and transporters screened at 10 μM) and was found to only significantly bind two targets (sodium channel site 2 and sigma 1) of the 68 assays conducted (no inhibition of radio ligand binding >50% at 10 μM).[45] Importantly, ML218 had no significant inhibition of L- and N-type calcium channels (17−49% inhibition @ 10 μM, respectively), K_{ATP} potassium channel (4% inhibition @ 10 μM), or hERG (48% inhibition @ 10 μM).[45]

ML218 was evaluated in our tier 1 in vitro DMPK panel.[46−49] In plasma protein binding studies (equilibrium dialysis), ML218 possessed good free fraction in both rat (f_u = 9.1%) and human (f_u = 3.3%). ML218 displayed minimal inhibition of P450 enzymes, including 3A4 (IC_{50} >30 μM), 2C9 (IC_{50} >30 μM), 1A2 (IC_{50} = 10.8 μM), and 2D6 (IC_{50} = 1.7 μM). Intrinsic clearance experiments in liver microsomes indicated that ML218 was highly cleared in rat (CL_{int} = 115 mL/min/kg), but low to moderately cleared in human liver

Scheme 1. Synthesis of [3.1.0] Analogues 26
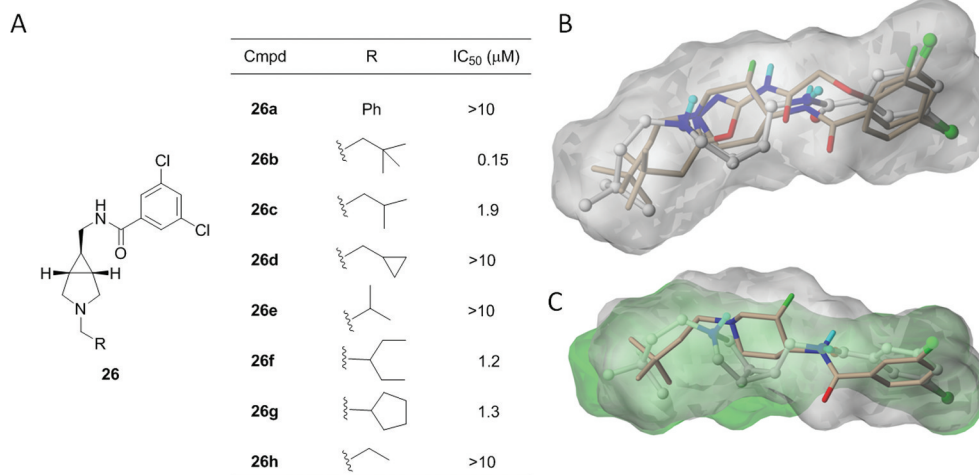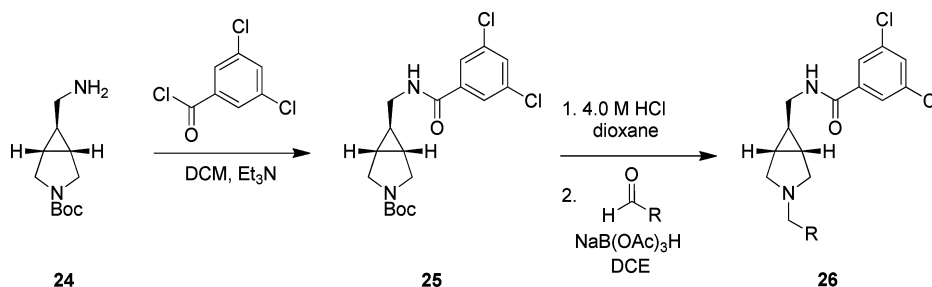

Figure 7. Second generation library of analogues of **18** focusing on a [3.1.0] core. (A) Structure and activities of [3.1.0] analogues **26a–h**. (B) Manual overlay of **18** and **26b** with Merck's **8**. (C) SurflexSim flexible alignment of **26b** (gray) with Merck's **8** (tan).
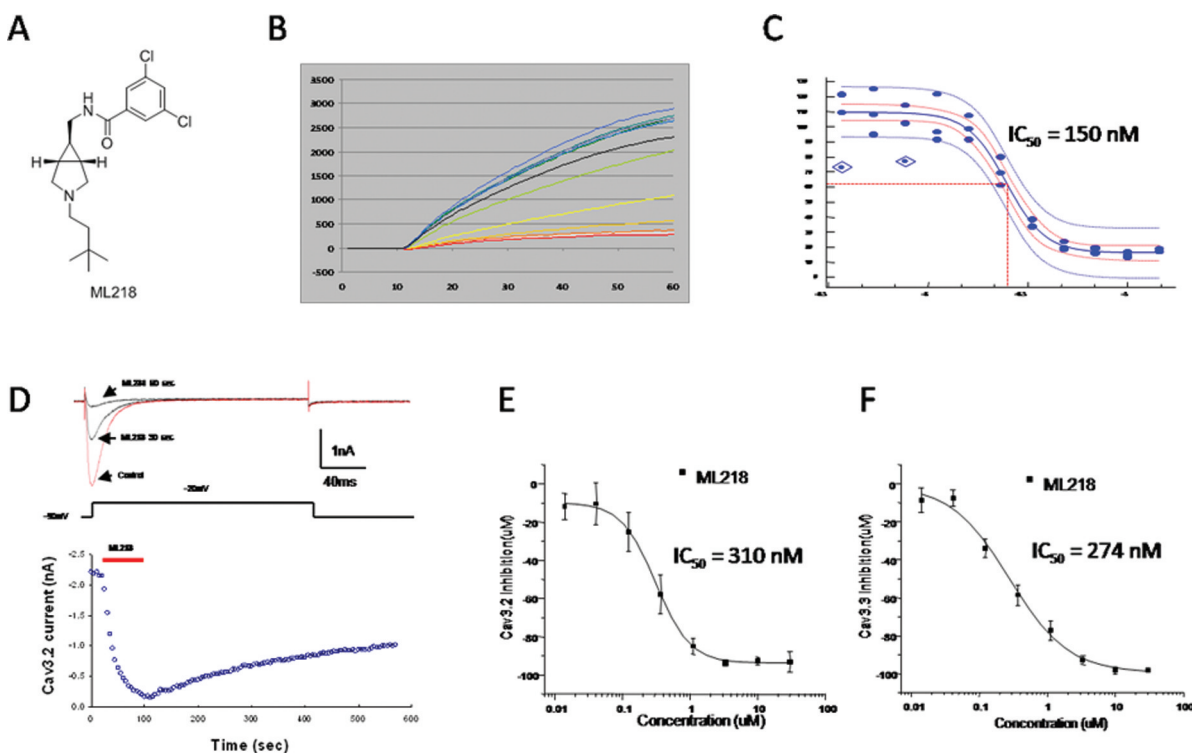

Figure 8. Dose–response curves for ML218 (**26b**). (A) Structure of ML218 (**26b**). (B) Raw fluorescence-based HTS assay traces. (C) CRC from fluorescence-based assay (IC_{50} = 150 nM). (D) Inhibition time-course of ML218. Ba^{2+} currents were elicited by pulse depolarized to −20 mV from a holding potential of −90 mV (200 ms, 0.2 Hz). The bath application of ML218 caused rapid inhibition and slow partially recovery after washout (n = 5). (E) $Ca_v3.2$ IonWorks Quattro (patch EP) CRC IC_{50} = 310 ± 15 nM. (F) $Ca_v3.3$ IonWorks Quattro (patch EP) CRC IC_{50} = 274 ± 53 nM.

microsomes (CL_{int} = 12.7 mL/min/kg). Results from an in vivo pharmacokinetic (PK) study in rats (1 mg/kg, IV) were consistent with the in vitro assessment, specifically with regards to an observed plasma clearance value (CLp = 56 mL/min/kg) that correlated with the predicted hepatic clearance value (CL_{HEP} = 43 mL/min/kg) obtained from rat liver microsomes. Noncompartmental PK analysis indicated ML218 had a mean residence time (MRT) of nearly 7 h, a value which was consistent with its terminal half-life ($t_{1/2}$ = 7 h). Importantly, ML218 was found to be highly brain penetrant with a brain$_{AUC}$/plasma$_{AUC}$ ratio of 7.4, implicating ML218's potential as an exceptional probe for CNS studies. The profile of ML218 is virtually identical to Merck's **8**, which showed modest rat PK parameters, but excellent dog, rhesus, and predicted human PK parameters.[29] Thus, the highly selective probe, ML218 (CID 45115620), possesses the requisite attributes (PK and CNS penetration) necessary to dissect the role of T-type Ca^{2+} channel inhibition in vitro and in vivo.

T-Type Ca^{2+} Channel Inhibitors and Parkinson's Disease. As mentioned earlier, T-type Ca^{2+} channels are strongly associated with rhythmic firing patterns in key brain regions within the CNS, such as in the olivocerebellar system, and inhibitors do block tremor-rhythm generation, affording therapeutic potential for essential tremor.[13−16,28,29] This concept could also be extended to the basal ganglia circuit, where abnormal burst firing in the STN results in over-activation of the indirect pathway, leading to Parkinsonian tremors.[17−19] Almost two decades ago, Hassani and co-workers demonstrated that 6-hydroxydopamine (6-OHDA) lessioned rats showed increased incidence of burst firing in the STN than control animals.[17] It is now well established that modification from a single-spike activity to a mixed bursting mode discharge pattern in STN neurons is one of the major hallmarks of Parkinsonism in rats and primates. Moreover, both high-frequency stimulation (HFS) and/or surgical resection of the STN ameliorates motor disturbances in Parkinson's disease (PD) patients, and significantly, the burst-firing mode of STN neurons can be attributed to both T- and L-type Ca^{2+} currents.[17−19] In a series of papers from Merck, both **7** and **8** were efficacious in dose−response on reversing harmaline-induced essential tremor, which led them to evaluate **8** in the haloperidol-induced catalepsy model of PD.[28,29] Here, a 10 mg/kg oral dose significantly reduced haloperidol-induced catalepsy, but there was no internal control by which to gauge the efficacy. To date, little has been done to thoroughly study T-type Ca^{2+} channel inhibitors as potential therapeutics for PD.

Electrophysiology Studies with ML218 in STN Neurons. Previous studies suggest that the burst-firing mode of STN neurons can be attributed to both T- and L-type Ca^{2+} currents.[17−19] Thus, we examined the effect of ML218 on the T-type calcium current, low threshold spike (LTS), and rebound burst activity in STN neurons (Figures 9−11). In a voltage clamp experiment, bath application of 3 μM ML218 significantly reduced the T-type Ca^{2+} current by ∼45% (Figure 9). Conversely, in a current clamp mode, 3 μM ML218 inhibited >50% of LTS amplitude, which was triggered by returning of a hyperpolarizing current pulse (−160 pA) in STN neurons (Figure 10). Similarly, 3 μM ML218 depressed >60% of rebound burst activity induced by intracellular injection of a hyperpolzarizing current (−100 pA) followed by a depolarizing current (−20 pA) in STN neurons (Figure 11). Together, these data suggest T-type Ca^{2+} channel inhibitors are an attractive therapeutic target for PD to regulate the abnormal burst firing
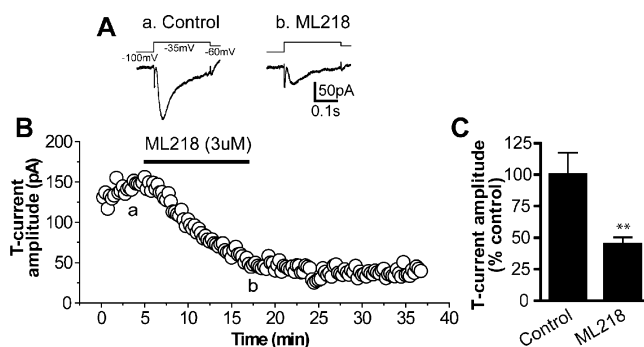

Figure 9. ML218 inhibits T-type calcium currents in STN neurons. (A) Averaged traces of T-currents (lower) elicited by a voltage clamp protocol (upper) in control (a) and after application of 3uM ML218 (b) in a voltage clamp experiment. (B) Time course of T-current amplitude before and after application of 3 uM ML218 from the same cell as in (A). (a) and (b) indicate the time points at which averaged traces were taken. (C) Bar graph summarizes group data showing ML218 inhibits T-currents in STN neurons (45.1 ± 5.1% of the control value, n = 7, **p < 0.005). Note that the inhibition persists 20 min after washout of ML218.
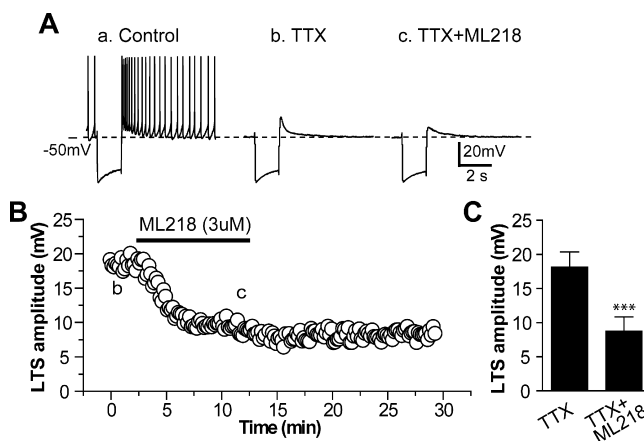

Figure 10. ML218 inhibits low threshold spike (LTS) in STN neurons. (A) Representative voltage responses to intracellular injection of a hyperpolarizing current pulse (−160 pA) in control (a), in the presence of 0.5 uM TTX (b), and combination of 0.5 uM TTX and 3 uM ML218 (c) from a current clamp experiment, showing the typical rebound burst firing following the termination of hyperpolarizing current pulse in control (a), pharmacologically isolated LTS in the presence of TTX (b), and inhibition of LTS by ML218 (c). (B) Time course of the effect of ML218 on amplitude of LTS obtained from the same STN neuron as in (A). (b) and (c) indicate the time points at which sample traces were taken. (C) Bar graph summarizes the group data showing ML218 inhibits the amplitude of LTS (8.7 ± 2.1 mV with ML218, compared to 18.1 ± 2.2 mV in control, n = 5, ***p < 0.0001).

in the STN, and therefore are able to reduce signaling in the indirect pathway of the basal ganglia circuit.

In Vivo Efficacy of ML218 in the Haloperidol-Induced Catalepsy Model of PD. In our PD programs, haloperidol-induced catalepsy is our first tier pharmacodynamic model to access therapeutic utility for PD.[49−51] In this model, a cataleptic state is induced by the administration of the dopamine antagonist haloperidol. Test compounds are then added, and potential anti-Parkisonian efficacy is based on a reversal of the cataleptic state.[49−51] As a control, we employ an A_{2A} antagonist, as previous studies have shown that selective A_{2A} antagonists produce robust
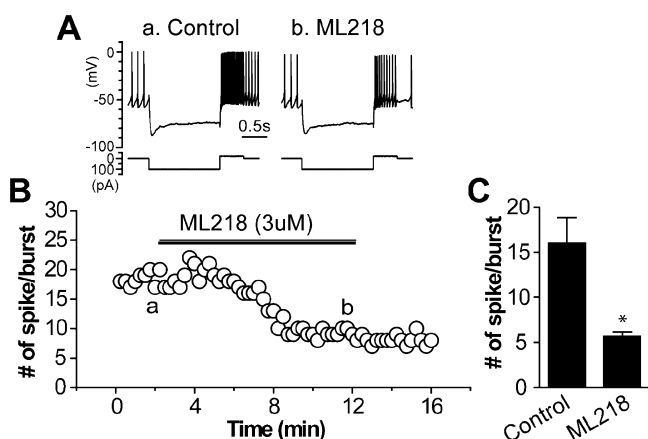
Figure 11. ML218 reduces rebound burst activity in STN neurons. (A) Representative voltage responses (upper) to intracellular injection of hyperpolarizing (−100 pA) followed by depolarizing (+20 pA) current pulses (lower) in control and after application of 3uM ML218 from a current clamp experiment. (B) Time course of the number of rebound spikes during the depolarizing current pulse before and after application of 3 uM ML218 from the same cell as in (A). (a) and (b) indicate the time points at which sample traces were taken. (B) Bar graph summarizes the group data showing ML218 reduces the number of rebound spikes in STN neurons (5.7 ± 0.5 spikes/burst with ML218, compared to 16.0 ± 2.8 spikes/burst in control, $n = 6$, *$p < 0.05$).

anti-Parkinsonian-like effects in animal models of dopamine depletion as well as in recent clinical trials with PD patients, when given alone or in combination with L-DOPA.[52] As shown in Figure 12A, Merck's **8**[29] at 10, 30, and 56.6 mg/kg i.p. reversed cataleptic behavior in rats induced by a 0.75 mg/kg dose of haloperidol, and this is comparable to a 56.6 mg/kg oral dose of an A_{2A} inhibitor. By way of comparison, ML218 at doses of 1, 3, 10, and 30 mg/kg p.o. reversed cataleptic behavior in rats induced by a 0.75 mg/kg dose of haloperidol, and this is comparable to a 56.6 mg/kg p.o. dose of an A_{2A} inhibitor (Figure 12B). Notably, the reversal with orally dosed ML218 approached the efficacy of a 56.6 mg/kg p.o. dose of the A_{2A} inhibitor.[52] Taken together with

the electrophysiology data in the STN, these experiments confirmed and validated inhibition of T-type Ca^{2+} channels as a therapeutic target for PD. Moreover, free brain and plasma concentrations of ML218 increased in a dose proportional manner across the dose range (3 mg/kg: [plasma] = 98 nM, [brain] = 1.66 μM; 10 mg/kg: [plasma] = 282 nM, [brain] = 5.03 μM; 30 mg/kg: 1.2 μM, [brain] = 17.7 μM)[53] with no alterations in brain/plasma ratios (average brain$_{AUC}$/plasma$_{AUC}$ of 16.9).

In summary, an MLPCN high-throughput screen (HTS) was conducted to identify novel T-type Ca^{2+} channel inhibitors free from IP constraints for use by the biomedical community to study T-type Ca^{2+} channels. While the HTS provided numerous hits, these compounds could not be optimized to the required level of potency to be appropriate tool compounds. Therefore, a scaffold hopping approach, guided by SurflexSim,[44] ultimately afforded ML218 (CID 45115620), a selective T-type Ca^{2+} ($Ca_v3.1$, $Ca_v3.2$, $Ca_v3.3$) inhibitor ($Ca_v3.2$, IC_{50} = 150 nM in Ca^{2+} flux; $Ca_v3.2$ IC_{50} = 310 nM and $Ca_v3.3$ IC_{50} = 270 nM in patch clamp electrophysiology) with good DMPK properties, acceptable in vivo rat PK, and excellent brain levels. Electrophysiology studies in STN neurons demonstrated robust effects of ML218 on the inhibition of T-type calcium current, inhibition of low threshold spike, and rebound burst activity. ML218 was found to be orally efficacious in a dose-dependent manner in a preclinical PD model, haloperidol-induced catalepsy, and comparable to clinically validated A_{2A} antagonism. Based on the overactive, indirect pathway in the basal ganglia circuitry in Parkinson's disease (PD), the effects of ML218 in STN neurons and in an in vivo PD model suggest a therapeutic role for T-type Ca^{2+} channel inhibitors. Thus, ML218 is a powerful new probe to study T-type Ca^{2+} function in vitro and in vivo, and, as all MLPCN probes, is freely available upon request. Current efforts are focused on the exploring the efficacy of ML218 in additional preclinical PD models, comparing the effects of voltage-dependent and voltage-independent T-type Ca^{2+} channel inhibitors, and these data will be reported in due course.
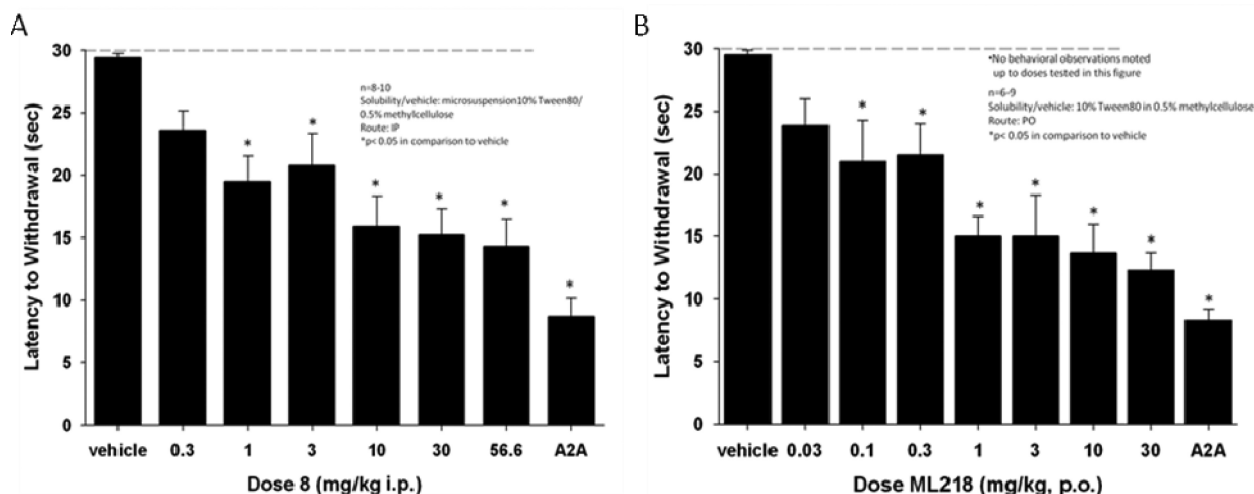

Figure 12. T-Type Ca^{2+} channel antagonist **8** and ML218 produce a dose-dependent reversal of haloperidol (0.75 mg/kg, i.p.)-induced catalepsy in rats. (A) For comparison, the effects of increasing dose of **8** (i.p.) were compared to a top dose (56.6 mg/kg p.o.) of a previously published A_{2A} antagonist from Neurocrine. (B) Comparison of the effects of increasing dose of ML218 (p.o.) to the Neurocrine A_{2A} antagonist at 56.6 mg/kg (p.o.). Catalepsy was measured as the latency to withdraw the forepaws from a horizontal bar with a cutoff of 30 s. Bar graphs represent the means ± SEM of either 6−10 rats/treatment group (*$p < 0.05$ versus the vehicle control group by Dunnett's test).

■ METHODS

Chemical Synthesis and Purification. All ^{1}H and ^{13}C NMR spectra were recorded on a Bruker AV-400 (400 MHz) or Bruker AV-NMR (600 MHz) instrument. Chemical shifts are reported in ppm relative to residual solvent peaks as an internal standard set to δH 7.26 or δC 77.0 (CDCl$_3$) and δH 3.31 or δC 49.0 (CD$_3$OD). Data are reported as follows: chemical shift, multiplicity (s = singlet, d = doublet, t = triplet, q = quartet, br = broad, m = multiplet), integration, coupling constant (Hz). IR spectra were recorded as thin films and are reported in wavenumbers (cm^{-1}). Low resolution mass spectra were obtained on an Agilent 1200 LCMS instrument with electrospray ionization. High resolution mass spectra were recorded on a Waters Qtof-API-US plus Acquity system. The value Δ is the error in the measurement (in ppm) given by the equation $\Delta = [(M_E - M_T)/M_T] \times 106$, where M_E is the experimental mass and M_T is the theoretical mass. The HRMS results were obtained with ES as the ion source and leucine enkephalin as the reference. Optical rotations were measured on a Perkin-Elmer-341 polarimeter. Analytical thin layer chromatography was performed on 250 μM silica gel 60 F254 plates. Visualization was accomplished with UV light, and/or the use of ninhydrin, anisaldehyde, and ceric ammonium molybdate solutions followed by charring on a hot-plate. Chromatography on silica gel was performed using Silica Gel 60 (230−400 mesh) from Sorbent Technologies. Analytical HPLC was performed on an Agilent 1200 analytical LCMS instrument with UV detection at 214 and 254 nm along with ELSD detection. Solvents for extraction, washing, and chromatography were HPLC grade. All reagents were purchased from Aldrich Chemical Co. and were used without purification. All polymer-supported reagents were purchased from Biotage, Inc. Flame-dried (under vacuum) glassware was used for all reactions. All reagents and solvents were commercial grade and purified prior to use when necessary. Mass spectra were obtained on a Micromass Q-Tof API-US mass spectrometer was used to acquire high-resolution mass spectrometry (HRMS) data.

3,5-Dichloro-N-((3-(3,3-dimethylbutyl)-3-azabicyclo[3.1.0]hexan-6-yl)methyl)benzamide (ML218). tert-Butyl 6-((3,5-Dichlorobenzamido)methyl)-3 azabicyclo[3.1.0]hexane-3-carboxylate (16). To a solution of exo-3-Boc-6-aminomethyl-3-azabicyclo[3.1.0]-hexane (1.0 equiv) and triethylamine (1.0 equiv) in CH$_2$Cl$_2$ at 0 °C was added a solution of 3,5-dichlorobenzoyl chloride (1.0 equiv) in CH$_2$Cl$_2$. The reaction stirred at 0 °C for approximately 4 h. The mixture was then concentrated in vacuo and purified by reverse phase chromatography (MeCN/H$_2$O/0.1% TFA) to afford the product as a white solid (93% yield). ^{1}H NMR (400 MHz, CD$_3$OD) δ (ppm): 7.83 (d, J = 1.92 Hz, 2H); 7.66 (t, J = 1.88 Hz, 1H); 3.57 (m, 2H); 3.35 (m, 4H); 1.60 (m, 2H); 1.46 (s, 9H); 0.90 (m, 1H). ^{13}C NMR (125 MHz, CD$_3$OD) δ (ppm): 167.96, 157.61, 139.75, 137.33, 133.02, 127.99, 81.86, 43.65, 29.56, 24.46, 24.02, 23.23. HRMS calcd for C$_{18}$H$_{22}$Cl$_2$N$_2$O$_3$, 385.1087 [M+H]; found, 385.1089. To a vial containing *tert*-butyl 6-((3,5-dichlorobenzamido)methyl)-3-azabicyclo[3.1.0]hexane-3-carboxylate **16** was added 4.0 M HCl in dioxane. This mixture was allowed to stir at room temp for 2 h. The reaction was then concentrated in vacuo and purified by reverse phase chromatography (MeCN/H$_2$O/0.1% TFA) to afford the product as a white solid (95% yield). ^{1}H NMR (400 MHz, CD$_3$OD) δ (ppm): 7.82 (d, J = 1.92 Hz, 2H); 7.68 (m, 1H); 3.45 (s, 4H); 3.34 (m, 2H); 1.90 (m, 2H); 1.21 (m,1H). ^{13}C NMR (100 MHz, CD$_3$OD) δ (ppm): 168.04, 163.95, 139.57, 137.40, 133.17, 127.97, 43.02, 23.35, 22.48. HRMS calcd for C$_{13}$H$_{14}$Cl$_2$N$_2$O, 285.0563 [M+H]; found, 285.0566.

3,5-Dichloro-N-((3-(3,3-dimethylbutyl)-3-azabicyclo[3.1.0]hexan-6-yl)methyl)benzamide (ML218). To a solution of 3,3-dimethylbutyraldehyde (1.0 equiv) in CH$_2$Cl$_2$ was added a solution of N-(3-azabicyclo[3.1.0]hexan-6-ylmethyl)-3,5-dichlorobenzamide (1.0 equiv) in CH$_2$Cl$_2$ followed by addition of polymer-supported sodium triacetoxyborohydride (1.2 equiv). The reaction was left to stir overnight at room temperature after which the mixture was filtered through a pad of Celite eluting with CH$_2$Cl$_2$ and concentrated in vacuo resulting in a crude oil which was then purified by reverse phase chromatography (MeCN/H$_2$O/0.1% TFA) to afford the product as an off-white solid (88% yield). ^{1}H NMR (400 MHz, CDCl$_3$) δ (ppm):

7.78 (d, J = 1.82 Hz, 2H); 7.57 (br, 1H); 7.42 (ap. t, J = 1.76 Hz, 1H); 3.64 (d, J = 10.56 Hz, 2H); 3.32 (t, J = 5.98 Hz, 2H); 2.95−2.83 (m,4H); 1.95 (m, 1H); 1.74 (s, 2H); 1.62 (m, 2H); 0.88 (s, 9H). ^{13}C NMR (100 MHz, CD$_3$OD) δ (ppm): 165.41, 137.46, 135.50, 131.46, 126.36, 55.69, 53.11, 41.94, 39.42, 30.07, 29.44, 21.71. HRMS calcd for C$_{19}$H$_{26}$Cl$_2$N$_2$O, 369.1500 [M+H]; found, 369.1501.

Calcium Mobilization Assays (T-Type Calcium Channel Cell-Based FDSS Ca^{2+} flux Assay). This protocol was employed for both the high-throughput screen as well as the primary assay. Cells were routinely cultured in D-MEM/F12 (Gibco 11330-032) supplemented with 10% heat-inactivated FBS (Sigma F2442), 0.5% sodium pyruvate (Gibco 11360), and 1 mg/mL G418 (Cellgro 30-234-CR) and then plated by the addition of 20 μL/well of 1000 cells/μL suspended in D-MEM/F12 (Gibco 11330−032) supplemented with 10% heat-inactivated FBS (Sigma F2442) and 0.5% sodium pyruvate (Gibco 11360). Cells were then incubated overnight at 37 °C and 5% CO$_2$. Medium was then removed with ELx405 and replaced with 20 μL/well of assay buffer (140 mM NaCl, 5 mM KCl, 1 mM MgCl$_2$, 0.5 mM CaCl$_2$, 10 mM glucose, 10 mM HEPES pH 7.3). Then 20 μL/well dye loading solution was added (4.6 μM Fluo-4 a.m. with 0.02% w/v Pluronic F-127 in Assay Buffer) with Combi and incubated 60 min at room temperature (RT). We prepared 2× compound plates by transferring 80 nL/well from stock plates containing compounds at 10 mM in DMSO to compound daughter plates and added 40 μL/well assay buffer using Combi. Negative (vehicle) control and positive control wells are 0.2% DMSO in assay buffer and EC$_{80}$ of **8** in assay buffer, respectively, in every other well of columns 1−2, 23−24. We replaced dye loading solution with 20 μL/well of assay buffer using ELx405 and then loaded cell plates onto a Hamamatsu FDSS 6000 kinetic imaging plate reader. Then, fluorescence was measured for 10 s at 1 Hz to establish baseline, followed by the addition of 20 μL/well test compounds from daughter plates; data collection continued for 50 s at 1 Hz. Plates were then removed from FDSS and incubated for 20 min at RT. Plates were reloaded to FDSS and data collection resumed at 1 Hz. After 10 s, we added 10 μL/well 5× stimulus buffer (140 mM NaCl, 5 mM KCl, 1 mM MgCl$_2$, 50 mM CaCl$_2$, 5 mM glucose, 10 mM HEPES pH 7.3) and continued collecting data for 2 min. Ratio readout was calculated as F/F_0 to normalize the data and reduce the waveform data to reflect the maximum normalized fluorescence/well. We calculated the average and standard deviation for negative and positive controls in each plate, as well as Z′.

Ca$_v$3.2 and Ca$_v$3.3 Calcium Channel IonWorks Electrophysiology Assays. Ca$_v$3 channel activity was examined in electrophysiological assays using the population patch clamp mode on the Ionworks Quattro (MDC, Sunnyvale, CA), an automated patch clamp instrument. The HEK293 cells stably expressing Ca$_v$3.2 and Ca$_v$3.3 channels were freshly dislodged from flasks and dispensed into a 384-well population patch clamp (PPC) plate, separately. The cell plating density was 7000 cells/well suspended in the extracellular solution, composed of (in mM) 137 NaCl, 4 KCl, 1 MgCl$_2$, 1.8 CaCl$_2$, 10 HEPES, and 10 glucose, pH 7.4 adjusted with NaOH. After dispensing, seal resistance of cells was measured for each well and cells were perforated by incubation with 50 μg/mL amphotericin B (Sigma, St. Louis, MO) on the intracellular side, which was dissolved in the internal solution composed of (in mM) 40 KCl, 100 K-Gluconate, 1 MgCl$_2$, 5 HEPES, 2 mM CaCl$_2$, pH 7.2 adjusted with KOH. The channel activity was then measured with the recording protocol as described below. Leak currents were linearly subtracted by extrapolating the current elicited by a 100 ms step to −110 mV from a holding potential of −100 mV. During the voltage pulse protocol, cells were held at −100 mV, followed by a depolarization step to −30 mV for 1 s, and then back to −90 mV. The currents were measured at the peak of the inward currents before and after the application of compounds for 3 min. Only cells with a current amplitude greater than 200 pA at −30 mV and a seal resistance of >30 MΩ were included in the data analysis. Compound effects were assessed by the percentage changes in the inward currents, which were calculated by dividing the difference of current amplitude between pre- and postcompound recordings by the respective precompound currents in the same well.

No corrections for liquid junction potentials were applied. The current signal was sampled at 0.625 kHz.

Brain Slice Preparation. Sprague−Dawley rats (P16-P22; Charles River, Wilmington, MA) were anesthetized with isoflorane and brains were rapidly removed from skulls and submerged in ice-cold cutting solution composed of the following (in mM): 200 glucose, 2.5 KCl, 8 $MgSO_4$, 0.5 $CaCl_2$, 1.25 NaH_2PO_4, 26 $NaHCO_3$, and 10 D-glucose, oxygenated with 95% O_2/5% CO_2. Parasagital brain slices (290−300 μm) containing the STN were cut using a Vibratome 3000 (Vibratome, St. Louis, MO). Slices were incubated in oxygenated artificial cerebrospinal fluid (ACSF) at 32 °C for 30 min and then maintained at room temperature afterward until transferred to a recording chamber. The recording chamber was continuously perfused with oxygenated ACSF containing (in mM) 126 NaCl, 2.5 KCl, 2.0 $CaCl_2$, 1.3 $MgSO_4$, 1.25 NaH_2PO_4, 26 $NaHCO_3$, and 10 D-glucose.

Brain Slice Electrophysiology. Whole cell recordings were made from visually identified STN neurons under an Olympus BX50WI upright microscope (Olympus, Lake Success, NY). A low-power objective (4×) was used to identify the brain region, and a 40× water immersion objective coupled with Hoffman optics was used to visualize the individual STN neurons. Patch pipettes were prepared from borosilicate glass (Sutter Instruments, Novato, CA) using a Narishige puller (model PP-830; Narishige International USA, East Meadow, NY) and had resistance of 3−4 MΩ when filled with the following intracellular solutions. For current-clamp recordings, the intracellular solution contained (in mM), 120 K-MeSO_4, 1 $MgCl_2$, 0.1 $CaCl_2$, 10 HEPES, 1 EGTA, 12 phosphocreatine, 2 Mg-ATP, and 0.4 Na_2-GTP. The pH of the pipet solution was adjusted to 7.3 with 1 M KOH, and osmolarity was adjusted to 290−295. For the voltage clamp recordings, the intracellular solution contained the following (in mM): 123 Cs-methanesulphonate, 10 TEA-Cl, 2 NaCl, 10 HEPES, 0.1 EGTA, 5 QX-315, 4 Mg-ATP and 0.3 Na_2-GTP. The pH was adjusted to 7.3 with 1 M CsOH, and osmolarity was adjusted to 290−295. Whole cell current and voltage signals were amplified using an Axon Multiclamp 700B amplifier (Molecular Devices, Sunnyvale, CA). Voltage or current commands, the digitization and acquisition of membrane potentials or currents were done using Clampex 9.2/ Digidata 1332 system (Molecular Devices, Sunnyvale, CA). In voltage clamp experiments, T-type calcium currents in STN neurons were isolated from voltage-gated sodium currents and high-voltage-gated calcium currents by including 0.5 uM tetrodotoxin (TTX) in the perfusate and applying the following voltage clamp protocol: a 400 ms hyperpolarization prepulse to −100 mV followed by a 300 ms depolarization test pulse from a holding potential of −60 mV. The amplitude of the test pulse was determined for each cell using depolarizing voltage steps in 5 mV increments from −100 mV until maximal T-type current amplitude was observed (typically −35 to −30 mV). Leakage subtraction was performed online using a P/4 protocol. In current clamp experiments, low threshold spike (LTS) was elicited by the termination of a hyperpolarizing current pulse (typically −150 to −160 pA, 1.5 s in duration) from zero current injection. Rebound burst activity was evoked by a hyperpolarizing current pulse (typically −100 pA, 1.5 s in duration) followed by a depolarizing current push-pulse (+20 pA, 0.5 s in duration) from zero current injection. ClampFit (Molecular Devices, Sunnyvale, CA) and Origin (OriginLab Corp, Northampton, MA) were used for data analysis. Group data were presented as mean ± SEM. The t test was used for statistical analysis, and $p < 0.05$ was considered to be significant.

Drug Metabolism Methods. *In Vitro.* Protein binding of ML218 was determined in rat plasma via equilibrium dialysis employing Single-Use RED Plates with inserts (ThermoFisher Scientific, Rochester, NY). Briefly, plasma (220 μL) was added to the 96-well plate containing test article (5 μL) and mixed thoroughly. Subsequently, 200 μL of the plasma-test article mixture was transferred to the *cis* chamber (red) of the RED plate, with an accompanying 350 μL of phosphate buffer (25 mM, pH 7.4) in the *trans* chamber. The RED plate was sealed and incubated 4 h at 37 °C with shaking. At completion, 50 μL aliquots from each chamber were diluted 1:1 (50 μL) with either plasma (*cis*) or buffer (*trans*) and transferred to a new 96-well plate, at which time ice-cold acetonitrile (2 volumes) was

added to extract the matrices. The plate was centrifuged (3000 rpm, 10 min), and supernatants transferred to a new 96-well plate. The sealed plate was stored at −20 °C until LC/MS/MS analysis. The metabolism of ML218 was investigated in rat hepatic microsomes (BD Biosciences, Billerica, MA) using substrate depletion methodology (% test article remaining). A potassium phosphate-buffered reaction mixture (0.1 M, pH 7.4) of test article (1 μM) and microsomes (0.5 mg/mL) was preincubated (5 min) at 37 °C prior to the addition of NADPH (1 mM). The incubations, performed in 96-well plates, were continued at 37 °C under ambient oxygenation, and aliquots (80 μL) were removed at selected time intervals (0, 3, 7, 15, 25, and 45 min). Protein was precipitated by the addition of chilled acetonitrile (160 μL), containing glyburide as an internal standard (50 ng/mL), and centrifuged at 3000 rpm (4 °C) for 10 min. Resulting supernatants were transferred to new 96-well plates in preparation for LC/MS/MS analysis. The in vitro half-life ($t_{1/2}$, min, eq 1), intrinsic clearance (CL_{int}, mL/min/kg, eq 2), and subsequent predicted hepatic clearance (CL_{hep}, mL/min/kg, eq 3) were determined employing the following equations:

$$t_{1/2} = \ln(2)/k \tag{1}$$

where k represents the slope from linear regression analysis (% test article remaining)

$$CL_{int} = (0.693/t_{1/2}) \tag{2}$$

(rxn volume/mg of microsomes) (45 mg microsomes/g of liver) (20 g of liver/kg body weight; scale-up factors of 20 (human) and 45 (rat))

$$CL_{hep} = \frac{Q \ CL_{int}}{Q + CL_{int}} \tag{3}$$

In Vivo. Male Sprague−Dawley rats ($n = 2$) weighing around 300 g were purchased from Harlan Laboratories (Indianapolis, IN) and implanted with catheters in the carotid artery and jugular vein. The cannulated animals were acclimated to their surroundings for approximately 1 week before dosing and were provided food and water ad libitum. ML218 was administered intravenously (IV) to rats via the jugular vein catheter in 20% DMSO/80% saline at a dose of 1 mg/kg and a dose volume of 1 mL/kg. Blood collections via the carotid artery were performed at predose, and at 2 min, 7 min, 15 min, 30 min, and 1 h, 2 h, 4 h, 7 h, and 24 h post dose. Samples were collected into chilled, EDTA-fortified tubes, and centrifuged for 10 min at 3000 rpm (4 °C), and resulting plasma was aliquoted into 96-well plates for LC/MS/MS analysis. All pharmacokinetic analysis was performed employing noncompartmental analysis. For oral exposure studies, measuring both systemic plasma and CNS tissue exposure, ML218 was administered (oral gavage) to fasted rats ($n = 2$) as suspensions in 10% Tween 80/0.5% methylcellulose at a dose of 10 mg/kg and in a dosing volume of 10 mL/kg; blood and whole brain samples were collected at 1.5 h post dose. Blood was collected into chilled, EDTA-fortified tubes, centrifuged for 10 min at 3000 rpm (4 °C), and stored at −80 °C until LC/MS/MS analysis. The brain samples were rinsed in PBS, snap frozen, and stored at −80 °C. Prior to LC/MS/MS analysis, brain samples were thawed to room temperature and subjected to mechanical homogenation employing a Mini-Beadbeater and 1.0 mm zirconia/silica beads (BioSpec Products). All animal studies were approved by the Vanderbilt University Medical Center Institutional Animal Care and Use Committee. The animal care and use program is fully accredited by the Association for Assessment and Accreditation of Laboratory Animal Care, International.

Liquid Chromatography/Mass Spectrometry Analysis. In Vivo Experiments. ML218 was analyzed via electrospray ionization (ESI) on an AB Sciex API-4000 (Foster City, CA) triple-quadrupole instrument that was coupled with Shimadzu LC-10AD pumps (Columbia, MD) and a Leap Technologies CTC PAL autosampler (Carrboro, NC). Analytes were separated by gradient elution using a Fortis C18 2.1 × 50 mm, 3.5 μm column (Fortis Technologies Ltd., Cheshire, U.K.) thermostatted at 40 °C. HPLC mobile phase A was 0.1% NH_4OH (pH unadjusted), and mobile phase B was acetonitrile.

The gradient started at 30% B after a 0.2 min hold and was linearly increased to 90% B over 0.8 min, held at 90% B for 0.5 min, and returned to 30% B in 0.1 min followed by a re-equilibration (0.9 min). The total run time was 2.5 min, and the HPLC flow rate was 0.5 mL/min. The source temperature was set at 500 °C, and mass spectral analyses were performed using multiple reaction monitoring (MRM) utilizing a turbo-ionspray source in positive ionization mode (5.0 kV spray voltage). All data were analyzed using AB Sciex Analyst 1.4.2 software.

In Vitro Experiments. ML218 was analyzed similarly to that described above (in vivo) with the following exceptions: LC/MS/MS analysis was performed employing a TSQ Quantum^{ULTRA} instrument that was coupled to a ThermoSurveyor LC system (Thermoelectron Corp., San Jose, CA) and a Leap Technologies CTC PAL autosampler (Carrboro, NC). Chromatographic separation of analytes was achieved with an Acquity BEH C18 2.1 × 50 mm, 1.7 μm column (Waters, Taunton, MA).

Plasma-Brain Exposure Profile PK Study. ML218 was dissolved in sterile water at the concentration of 5 mg/mL (base form) and administered intraperitoneally to male Sprague−Dawley rats weighing 225−250 g (Harlan Sprague−Dawley, Inc., Indianapolis, IN) at the dose of 10 mg/kg. The rat blood and brain were collected at 0.5, 1, 2, 4, and 8 h. Animals were euthanized and decapitated, and the brains were removed, thoroughly washed with cold phosphate buffered saline, and immediately frozen on dry ice. Trunk blood was collected in EDTA Vacutainer tubes, and plasma was separated by centrifugation and stored at −80 °C until analysis. Three animals were used for each time point.

On the day of analysis, frozen whole-rat brains were weighed and homogenized in 1:3 (w/w) volumes of ice-cold phosphate buffered saline (pH 7.4). The sample extraction of plasma (100 μL) and brain homogenate (250 μL) was performed by a method based on protein precipitation, using three volumes of cold acetonitrile containing 0.1% formic acid and an internal standard (VU-178) having final concentration of 50 ng/mL. Extracts were vortex mixed for 5 min followed by centrifugation at 14 000 rpm for 10 min.

The supernatants of plasma and brain homogenate extracts were analyzed by means of HPLC/MS/MS, using a ThermoFinnigan TSQ Quantum Access (Thermo Fisher Scientific, Waltham, MA) mass spectrometer in positive ion mode. The chromatographic separation was achieved on an Acquity UPLC BEH C18 column (1.7um; 2.1 × 50 mm) at a flow rate of 0.8 mL/min. The gradient program was used with the mobile phase, combining solvent A (95:5, 0.1% formic acid in water/acetonitrile) and solvent B (95:5, acetonitrile/0.1% formic acid in water) as follows: 20% B for 0−0.5 min, 20−95% B for 0.5−1 min, 95% B for 1−2 min, 95−20% B for 2−2.2 min, and finally equilibration for 2.8 min before injection of next sample. The column temperature was set at 50 °C. The software Xcalibur version 2.0 was used to control the instrument and collect data. The electrospray ionization source was fitted with a stainless steel capillary (100 μm i.d.). Nitrogen was used as both the sheath gas and the auxiliary gas. The ion transfer tube temperature was 300 °C. The spray voltage, tube lens voltage, and pressure of sheath gas and auxiliary gas were optimized to achieve maximal response using the test compounds mixing with the mobile phase A (50%) and B (50%) at a flow rate of 0.8 mL/min. Collision-induced dissociation was performed on ML218 and internal standard under 1.0 mTorr of argon. Selected reaction monitoring was carried out using the transitions from m/z 320 to 148 for ML218 and m/z 310 to 223 for VU-178 (internal standard). The calibration curves were constructed, and linear response was obtained in the range of 10−2000 ng/mL by spiking known amounts of analytes in blank brain homogenates and plasma. The final PK parameters were calculated by noncompartmental analysis using WinNonlin software (version 5.1, Pharsight Inc.). Data analysis was carried out utilizing the GraphPad Prism 4.0 software package. Statistical analyses and nonlinear curve fits were carried out utilizing built in functions. Data are plotted as mean ± SEM unless otherwise specified. Experiments were conducted in accordance with the U.S. National Institutes of Health regulations of animal care and approved by the Institutional Animal Care and Use Committee, Vanderbilt University Medical Center. Subjects were housed in groups of two per cage in a large colony room under a 12 h light−dark cycle (lights on at 6:00 a.m.) with food and water provided ad libitum.

Haloperidol-Induced Catalepsy. Male Sprague−Dawley rats weighing between 275 and 299 g (Harlan Laboratories, Inc. Indianapolis, IN) were used for the behavioral studies and were housed under a 12 h light/dark cycle (lights on at 6:00 a.m., lights off at 6:00 p.m.) with free access to food and water. The experimental protocols, which were performed during the light cycle, were approved by the Institutional Animal Care and Use Committee of Vanderbilt University and conformed to the guidelines established by the National Research Council Guide for the Care and Use of Laboratory Animals. Rats were administered haloperidol (0.75 mg/kg, i.p., dissolved in 8.5% lactic acid) 60 min prior to vehicle (10% Tween 80 in 0.5% methylcellulose) or ML218 (0.1−30 mg/kg). After an additional 30 min pretreatment interval, all rats were assessed in the catalepsy model. Catalepsy was measured by placing the forepaws of each rat gently onto a horizontal bar 6 cm from the testing surface with the body positioned at an angle of ∼45° to the testing surface. The latency in seconds required for the rat to remove one or both forepaws from the bar was measured with a testing cutoff of 30 s.

■ ASSOCIATED CONTENT

Ⓢ Supporting Information

ML218 experimental details; SAR of analogues of **16**; additional DMPK data for ML218; NMR and LCMS data for ML218. This material is available free of charge via the Internet at http://pubs.acs.org.

■ AUTHOR INFORMATION

Corresponding Author

*Mailing address: Departments of Pharmacology and Chemistry, Vanderbilt Specialized Chemistry Center (MLPCN), Vanderbilt Center for Neuroscience Drug Discovery, Vanderbilt University Medical Center, Nashville, TN 37232-6600, USA. E-mail: craig.lindsley@vanderbilt.edu. Telephone: 615-322-8700. Fax: 615-343-6532.

Author Contributions

†These authors contributed equally to this work.

Author Contributions

Professors Lindsley, Weaver, Conn, Jones, Daniels, and Dawson oversaw and designed the chemistry, HTS, molecular pharmacology, behavioral pharmacology, DMPK, and modeling, respectively. Professor Thompson performed the haloperidol-induced catalepsy studies. Professor Xiang performed the electrophysiology studies. Professor Hopkins oversaw chemistry. Mr. Brogan performed synthetic chemistry. Mr. Schulte performed synthetic chemistry. Dr. Melancon performed synthetic chemistry and scaled-up key compounds for in vivo studies. Dr. Xie was the assay provider and coordinated the HTS and electrophysiology. Dr. Zou and Dr. Yang performed electrophysiology. Mr. Aldrich performed synthetic chemistry. Dr. Lewis and Mrs. Mi conducted the HTS. Mrs. Santomango, Mr. Byers, Mr. Morrison, and Ms. Brewer performed DMPK and bioanalytical studies. Dr. Yu, Dr. McManus, and Dr. Li performed the Cav$_{3.2/3.3}$ electrophysiology

■ ABBREVIATIONS:

IP, intellectual property; STN, subthalamic nucleus; HTS, high-throughput screen; PD, Parkinson's disease; VGCC, voltage-gated calcium channels; i.p., intraperioneal; p.o., oral dosing; LTS, low threshold spike; ZNS, zonisamide; GPCR, G protein-coupled receptor

■ REFERENCES

(1) Petegem, F. V., and Minor, D. L. Jr. (2006) The structural biology of voltage-gated calcium channel function and regulation. *Biochem. Soc. Trans. 34*, 887–893.

(2) Huguenard, J. R. (1998) Low-voltage-activated (T-type) calcium-channel genes identified. *Trends Neurosci. 21*, 451–452.

(3) Ertel, E. A., Campbell, K. P., Harpold, M. M., Hofmann, F., Mori, Y., Perez-Reyes, E., Schwartz, A., Snutch, T. P., Tanabe, T., Birnbaumer, L., Tsien, R. W., and Catterall, W. A. (2005) Nomenclature of voltage-gated calcium channels. *Neuron 25*, 533–535.

(4) Catterall, W. A., Perez-Reyes, E., Snutch, T. P., and Striessing, J. (2005) International Union of Pharmacology. XLVIII. Nomenclature and structure-function of voltage-gated calcium channels. *Pharmacol. Rev. 57*, 411–425.

(5) Catterall, W. A. (2000) Structure and regulation of voltage-gated Ca^{2+} channels. *Annu. Rev. Cell Dev. Biol. 16*, 521–555.

(6) Carbone, E., and Lux, H. D. (1984) A low voltage-activated, fully inactivating Ca channel in vertebrate sensory neurons. *Nature 310*, 501–502.

(7) Lacinova, L. (2004) Pharmacology of recombinant low-voltage activated calcium channels. *Curr. Drug Targets: CNS Neurol. Disord. 3*, 105–111.

(8) Talley, E. M., Cribbs, L. L., Lee, J. H., Daud, A., Perez-Reyes, E., and Bayliss, D. A. (1999) Differential distribution of three members of a gene family encoding low voltage-activated (T-type) calcium channels. *J. Neurosci. 19*, 1895–1911.

(9) Nelson, M. T., Todorovic, S. M., and Perez-Reyes, E. (2006) The role of T-type calcium channels in epilepsy and pain. *Curr. Pharm. Des. 12*, 2189–2197.

(10) Perez-Reyes, E. (2006) Molecular characterization of T-Type calcium channels. *Cell Calcium 40*, 89–96.

(11) Shin, H.-S., Cheong, E.-J., Choi, S., Lee, J., and Na, H. S. (2008) T-Tye Ca^{2+} channels as therapeutics in the nervous system. *Curr. Opin. Pharmacol. 8*, 33–41.

(12) Contreas, D. (2006) The role of T-channels in the generatin of thalamocortical rythyms. *CNS Neurol. Disord.: Drug Targets 5*, 571–585.

(13) Llinás, R., and Yarom, Y. (1981) Electrophysiology of mammalian inferior olivary neurones in vitro. Different types of voltage-dependent ionic conductances. *J. Physiol. 315*, 549–67.

(14) Wilms, H., Sievers, J., and Deuschl, G. (1999) Animal models of tremor. *Mov. Disord. 14*, 557–71.

(15) Miwa, H. (2007) Rodent models of tremor. *Cerebellum 6*, 66–72.

(16) Park, Y. G., Park, H. Y., Lee, C. J., Choi, S., Jo, S., and Choi, H. (2010) Ca(V)3.1 is a tremor rhythm pacemaker in the inferior olive. *Proc. Natl. Acad. Sci. U.S.A. 107*, 10731–10736.

(17) Hassani, O. K., Mouroux, M., and Feger, J. (1999) Increased subthalamic neuronal activity after nigral dopaminergic lesion independent of disinhibition via the globus pallidus. *Neuroscience 72*, 105–115.

(18) Hammond, C., Beurrier, C., Garcia, L., and Bioulac, B. (2002) Physiological and pathological patterns in subthalamic neurons related to Parkinson's disease. *Neurophysiology 34*, 96.

(19) Miwa, H., Koh, J., Kajimoto, Y., and Kondo, T. (2011) Effects of T-type calcium channel blockers on a parkinsonian tremor model in rats. *Pharmacol., Biochem. Behav. 97*, 656–659.

(20) Morita, S., Miwa, H., and Kondo, T. (2005) Effect of zonisamide on essential tremor: a pilot crossover study in comparison with arotinolol. *Parkinsonism Relat. Disord. 11*, 101–103.

(21) Broicher, T., Seidenbecher, T., Meuth, P., Munsch, T., Meuth, S. G., Kanyshkova, T., Pape, H.-C., and Budde, T. (2007) T-Current related effects of antiepileptic drugs and a Ca^{2}+ channel antagonist on thalamic relay and local circuit interneurons in a rat model of absence epilepsy. *Neuropharmacology 53*, 431–446.

(22) Leuranguer, V., Mangoni, M. E., and Nargeot, R. S. (2001) Inhibition of T-type and L-type calcium channels by mibefradil: physiologic and pharmacologic bases of cardiovascular effects. *J. Cardiovasc. Pharmacol. 37*, 649–661.

(23) Moosmang, S., Haider, N., Bruderl, B., Welling, A., and Hofmann, F. (2006) Antihypertensive effects of the putative T-type calcium channel antagonist mibefradil are mediated by the L-type calcium channel Cav1.2. *Circ. Res. 6*, 105–110.

(24) Tanaka, H., and Shigenobu, K. (2002) Efonidipine hydro-chloride: a dual blocker of L- and T-type Ca^{2+} channels. *Cardiovasc. Drug Rev. 20*, 81–92.

(25) Tytgat, J., Vereecke, J., and Carmeliet, E. (1996) Mechanism of L- and T-type Ca^{2+} channel blockade by flunarizine in ventricular myocytes of the guinea-pig. *Eur. J. Pharmacol. 296*, 189–197.

(26) Bancila, M., Copin, J. C., Daali, Y., Schatlo, B., Gasche, Y., and Bijlenga, P. (2011) Two structurally different T-type Ca 2+ channel inhibitors, mibefradil and pimozide, protect CA1 neurons from delayed death after global ischemia in rats. *Fundam. Clin. Pharmacol. 25*, 469–478.

(27) Giordanetto, F., Knerr, L., and Walberg, A. (2011) T-type calcium channels inhibitors: a patent review. *Exp. Opin. Ther. Patents 21*, 85–101.

(28) Shipe, W. D., Barrow, J. C., Yang, Z.-Q., Lindsley, C. W., Yang, F. V., Schlegel, K. S., Shu, Y., Rittle, K. E., Zrada, M. M., Bock, M. G., Hartman, G. D., Tang, C., Ballard, J. E., Kuo, Y., Adarayan, E. D., Prueksaritanont, Y., Uebele, V. N., Nuss, C. E., Connolly, T. M., Doran, S. M., Fox, S. V., Kraus, R. L., Marino, M. J., Graufelds, V. K., Vargas, H. M., Bunting, P. B., Hasbun-Manning, M., Evans, R. M., Koblan, K. S., and Renger, J. J. (2008) Design, synthesis and evaluation of novel 4-aminomethyl-4-fluoropiperidine as a T-Type Ca2+ antagonist. *J. Med. Chem. 51*, 3692–3695.

(29) Yang, Z.-Q., Barrow, J. C., Shipe, W. D., Schlegel, K. S., Shu, Y., Yang, F. V., Lindsley, C. W., Rittle, K. E., Bock, M. G., Hartman, G. D., Uebele, V. N., Nuss, C. E., Fox, S. V., Kraus, R. L., Doran, S. M., Connolly, T. M., Tang, C., Ballard, J. E., Kuo, Y., Adarayan, E. D., Prueksaritanont, Y., Zrada, M. M., Marino, M. J., DiLella, A. G., Reynolds, I. J., Vargas, H. M., Bunting, P. B., Woltman, M. M., Koblan, K. S., and Renger, J. J. (2008) Discovery of 1,4-substituted piperidines as potent and selective inhibitors of T-type calcium channels. *J. Med. Chem. 51*, 6471–6477.

(30) Barrow, J. C., Lindsley, C. W., Shipe, W. D., Yang, Z., and Wisnoski, D. D. (2010) 4-Fluoro-Piperdine T-Type Calcium Channel Antagonists. WO 0216841.

(31) Barrow, J. C., Lindsley, C. W., Shipe, W. D., and Yang, Z. (2010) 3-Fluoro-Piperdine T-Type Calcium Channel Antagonists. WO 0222387.

(32) Renger, T. S., Yang, Z. Q., Schlegel, K. S., Shu, Y., Mattern, C., Cube, R., Rittle, K. E., McGaughey, G. B., Hartman, G. D., Tang, C., Ballard, J., Kuo, Y., Prueksaritanont, T., Nuss, C. E., Doran, S. M., Fox, S. V., Garson, S. L., Yuxing, L., Kraus, R. L., Uebele, V. N., Renger, J. J., and Barrow, J. C. (2011) Pyridyl amides as potent inhibitors of T-type calcium channels. *Bioorg. Med. Chem. Lett. 21*, 1692–1696.

(33) Schlegel, K. S., Yang, Z. Q., Renger, T. S., Shu, Y., Cube, R., Rittle, K. E., Bondiskey, P., Bock, M. G., Hartman, G. D., Tang, C., Ballard, J., Kuo, Y., Prueksaritanont, T., Nuss, C. E., Doran, S. M., Fox,

S. V., Garson, S. L., Yuxing, L., Kraus, R. L., Uebele, V. N., Renger, J. J., and Barrow, J. C. (2010) Discovery and expanded SAR of 4,4-disubstituted quinazolin-2-ones as potent T-type calcium channel antagonists. *Bioorg. Med. Chem. Lett. 20*, 5147−5152.

(34) Dreyfus, F. M., Tscherter, A., Errington, A. C., Renger, J. J., Shin, H.-S., Uebele, V. N., Crunelli, V., Lambert, R. C., and Leresche, N. (2010) Selective T-type calcium channel block in thalamic neurons reveals channel redundancy and physiological impact of $I_{Twindow}$. *J. Neurosci. 30*, 99−109.

(35) Smith, E. M., Sorota, S., Kim, H. M., McKittrick, B. A., Nechuta, T. L., Bennett, C., Knuston, C., Burnett, D. A., Kieselgof, J., Tan, Z., Rindgen, D., Bridal, T., Zhou, X., Jia, Y.-P., Dong, Z., Mullins, D., Zhang, X., Priestly, T., Correll, C. C., Tulshian, D., Czarniecki, M., and Greenlee, W. J. (2010) T-type calcium channel blockers: spiro-piperidine azetidines and azetidinones—optimization, design and synthesis. *Bioorg. Med. Chem. Lett. 20*, 4602−4606.

(36) Choi, Y.-H., Baek, D. J., Lee, J. K., Pae, A. N., Cho, Y. S., and Min, S.-J. (2011) Facile synthesis and biological evaluation of 3,3-diphenylpropanoyl piperazines as T-type calcium channel blockers. *Bioorg. Med. Chem. Lett. 21*, 215−219.

(37) Hangeland, J. J., Cheney, D. L., Friends, T. J., Swartz, S., Levesque, P. C., Rich, A. J., Sun, L., Bridal, T. R., Adam, L. P., Normandin, D. E., Murugesan, N., and Ewing, W. R. (2008) Design and SAR of selective T-type calcium channel antagonists containing a biaryl sulfonamide core. *Bioorg. Med. Chem. Lett. 18*, 474−478.

(38) Gu, S. J., Lee, J. K., Pae, A. N., Chung, H. J., Rhim, H., Han, S. Y., Min, S.-J., and Cho, Y. S. (2010) Synthesis and biological evaluation of 1,4-diazepane derivatives as T-type calcium channel blockers. *Bioorg. Med. Chem. Lett. 20*, 2705−2708.

(39) Fritch, P. C., and Krajewski, J. (2010) Design, syntheses, and SAR of 2,8-diazaspiro[4.5]decanones as T-type calcium channel antagonists. *Bioorg. Med. Chem. Lett. 20*, 6375−6378.

(40) Lee, J. E., Koh, H. Y., Seo, S. H., Baek, Y. Y., Rhim, H., Cho, Y. S., and Pae, A. N. (2010) Synthesis and biological evaluation of oxazole derivatives as T-type calcium channel blockers. *Bioorg. Med. Chem. Lett. 20*, 4219−4222.

(41) For information on the MLSCN and MLPCN, see http://mli.nih.gov/mli/mlpcn/.

(42) Xie, X., Van Duesen, A. L., Vitko, I., Babu, D. A., Davies, L. A., Huynh, N., Cheng, H., Yang, N., Barrett, P. Q., and Perez-Reyes, E. (2007) Validation of high throughput screening assays against three subtypes of Ca(v)3 T-type channels using molecular and pharmacologic approaches. *Assay Drug Dev. Technol. 5*, 191−203.

(43) For information on the MLPCN, see the MLPCN database Pubchem (open access): http://pubchem.ncbi.nlm.nih.gov/.

(44) Jain, A. M. (2000) Morphological similarity: A 3D molecular similarity method correlated with protein-ligand recognition. *J. Comput.-Aided Drug Des. 14*, 199−213.

(45) For information on the Ricerca Lead Profiling Screen, see www.ricerca.com.

(46) Lindsley, C. W., Bates, B. S., Menon, U. N., Jadhav, S. B., Kane, A. S., Jones, C. K., Conn, P. J., Olsen, C. M., Winder, D. G., and Emmitte, K. A. (2011) (3-Cyano-5-fluorophenyl)biaryl non-competitive antagonists of mGlu$_5$: Discovery of a new tool compound with activity in mouse models of anxiety and addiction. *ACS Chem. Neurosci. 2*, 471−482.

(47) Wang, H.-R., Wu, M., Yu, H., Long, S., Stevens, A., Engers, D. W., Sakin, H., Daniels, J. S., Dawson, E. S., Hopkins, C. R., Lindsley, C. W., Li, M., and McManus, O. B. (2011) Selective inhibition of the $K_{ir}2$ family of inward rectifier potassium channels by a small molecule probe: the discovery, SAR and pharmacological characterization of ML133. *ACS Chem. Biol. 6*, 845−856.

(48) Reid, P. R., Bridges, T. M., Sheffler, D. A., Cho, H. P., Lewis, L. M., Days, E., Daniels, J. S., Jones, C. K., Niswender, C. M., Weaver, C. D., Conn, P. J., Lindsley, C. W., and Wood, M. R. (2011) Discovery and optimization of a novel, selective and brain penetrant M_1 positive allosteric modulator (PAM): the development of ML169, an MLPCN Probe. *Bioorg. Med. Chem. Lett. 21*, 2697−2701.

(49) Engers, D. W., Field, J. R., Le, U., Zhou, S., Bolinger, J. D., Zamorano, R., Blobaum, A. L., Jones, C. K., Jadhav, S., Weaver, C. D., Conn, P. J., Lindsley, C. W., Niswender, C. M., and Hopkins, C. R. (2011) Discovery, Synthesis, and SAR Development of a Series of *N*-(4-acetamido)-phenylpicolinamides as Positive Allosteric Modulators of Metabotropic Glutamate Receptor 4 (mGlu$_4$) with CNS Exposure in Rats. *J. Med. Chem. 54*, 1106−1110.

(50) Williams, R., Zhou, Y., Niswender, C. M., Luo, Q., Conn, P. J., Lindsley, C. W., and Hopkins, C. R. (2010) Re-exploration of the PHCCC scaffold: Discovery of improved positive allosteric modulators of mGluR4. *ACS Chem. Neurosci. 1*, 411−419.

(51) Niswender, C. M., Myers-Johnson, K. A., Weaver, C. D., Jones, C. K., Luo, Q., Rodriguez, A. L., Marlo, J. E., de Paulis, T., Thompson, A., Days, E., Nalywajko, N. T., Austin, C., Williams, M., Ayala, J. E., Williams, R., Lindsley, C. W., and Conn, P. J. (2008) Discovery, characterization and antiparkinsonian effect of novel positive allosteric modulators of metabotropic glutamate receptor 4. *Mol. Pharmacol. 74*, 1345−1358.

(52) Slee, D. H., Zhang, X., Moorjani, M., Lin, E., Lanier, M. C., Chen, Y., Reuter, J. K., Lechner, S. M., Markison, S., Malany, S., Joswig, T., Santos, M., Gross, R. S., Williams, J. P., Castro-Palomino, J. C., Crespo, M. I., Prat, M., Gual., S., Diaz, J.-L., Wen, J., O'Brien, Z., and Saunders, J. (2008) Identification of novel, water-soluble, 2-amino-*N*-pyrimidin-4-yl acetamides as A$_{2A}$ receptor antagonists with in vivo efficacy. *J. Med. Chem. 51*, 400−406.

(53) See the Supporting Information for full details.

742

dx.doi.org/10.1021/cn200090z | *ACS Chem. Neurosci.* 2011, 2, 730−742